Title

Supramolecular Hyaluronic Assembly with Aggregation-Induced Emission Mediated in Two Stages for Targeting Cell Imaging

Journal

ACS Medicinal Chemistry Letters, 11(4)

ISSN

1948-5875

Authors

Yang, Yang
Jin, Ya-Jun
Jia, Xin
et al.

Publication Date

2020-04-09

DOI

10.1021/acsmedchemlett.9b00559

Peer reviewed

ACS Medicinal Chemistry Letters

pubs.acs.org/acsmedchemlett Letter

Supramolecular Hyaluronic Assembly with Aggregation-Induced Emission Mediated in Two Stages for Targeting Cell Imaging

Yang Yang, Ya-Jun Jin, Xin Jia, Shi-Kuo Lu, Ze-Rui Fu, Yu-Xi Liu, and Yu Liu*

Cite This: *ACS Med. Chem. Lett.* 2020, 11, 451−456 Read Online

ACCESS | Metrics & More | Article Recommendations | Supporting Information

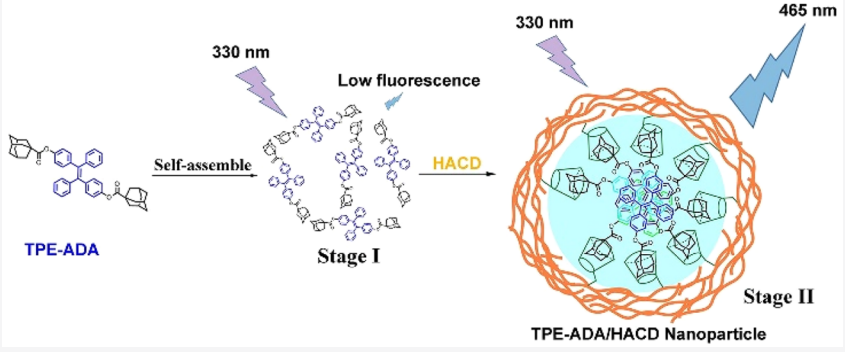

ABSTRACT: Supramolecular aggregation-induced emission (AIE) has become a research hotspot in cell imaging. Herein, supramolecular assembly with AIE effect was constructed in two stages, where adamantane modified tetraphenylethene self-assembly emitted weak fluorescence, and then after adding β-cyclodextrin modified hyaluronic acid, the formed nanoparticles enhanced AIE fluorescence for targeted cancer cell imaging.

KEYWORDS: *Supramolecular assembly, aggregation-induced emission, tetraphenylethene, hyaluronic acid, cell imaging*

Nowadays, supramolecular aggregation-induced emission (AIE) and its application in cell imaging have become the research focus in the field of supramolecular chemistry.[1,2] The phenomenon of AIE fluorescence, which exhibits negligible emission in dilute solution but emits intense fluorescence in aggregation or solid state, was first discovered by Ben Zhong Tang et al. in 2001.[3] The mechanism of AIE effect is the restriction of intramolecular rotations and inhibition of nonradiative decay.[4,5] In recent decades, AIE materials have gained more and more interest due to the superior features compared to conventional fluorescent reagents, such as high solid quantum yield and photostability, excellent biocompatibility, free of random blinking, and strong photobleaching resistance, which jointly facilitated applications of AIE materials on fluorescence imaging.[6,7] Among the variety of AIE materials, tetraphenylethene (**TPE**) with aggregation and fluorescence behaviors was considered as a candidate material used in fluorescent imaging at the subcellular, cellular, or tissue levels in noninvasive and high contrast manners due to its facile synthesis and easy modification.[8−11]

On the other hand, supramolecular aggregates with remarkable fluorescence and drug loading capability were frequently studied in recent years due to the easy fabrication using building blocks via supramolecular and amphiphilic interactions.[12−15] The traditional host−guest interaction between adamantane and β-cyclodextrin (β-CD) cavity had been employed for construction of numerous supramolecular architectures.[16−19] Moreover, hyaluronic acid (**HA**), a water-soluble acidic polysaccharide, is frequently used as the aggregation-inducing scaffold, AIE turn-on agent,[20,21] and targeting unit[22−24] due to its biocompatibility, biodegradability, easy modification, low toxicity, and specific targeting toward CD44 and RHAMM (receptor for HA-mediated motility) receptors overexpressed on the surface of cancer cells.[25−27] Therefore, **HA**-based supramolecular AIE assemblies possess great potential in fluorescence imaging applications. For instance, Qian Zhao et al.[28] fabricated tetraphenylethylene-bridged β-CD (TPECD) and adamantyl-grafted hyaluronic acids (HAAD), and formed spherical nanoparticles by mixing the two building blocks together. However, the rigid structure of TPECD grafted four bulk β-CDs is adverse to π stacking and molecular restriction of tetraphenylethene core; then the further enhancement of AIE fluorescence was not prominent for nanoparticles. Therefore, fluorescent doxorubicin was employed to be loaded into the

Received: November 29, 2019
Accepted: February 28, 2020
Published: February 28, 2020

https://dx.doi.org/10.1021/acsmedchemlett.9b00559
ACS Med. Chem. Lett. 2020, 11, 451−456

nanoparticles for cancer cell imaging. For another, Bang-Ping Jiang et al.[29] reported a novel multifunctional AIE nanoaggregate fabricated through electrostatic interactions between positive charged quaternary ammonium-modified **TPE** derivative and negative charged crude **HA**. The obtained nanoaggregate presented AIE turn-on fluorescence for targeted imaging of cancer cells. Nevertheless, the investigation of the aggregation strategy of **TPE** derivatives before and after adding host molecules (such as β-CD-modified hyaluronic acid (**HACD**)) at different stages and acquiring enhanced AIE effect is still rarely reported.

In this work, adamantane-modified tetraphenylethene (**TPE-ADA**) with two small adamantane groups and low solubility could self-assemble and emit low fluorescence in aqueous solution at the first stage. When **HACD** was added, supramolecular nanoparticles (**TPE-ADA/HACD**) were formed via the strong host−guest interaction. Then the hydrophobic **TPE** core in the nanoparticles would stack and emit strong AIE fluorescence at the second stage (Scheme 1).

Scheme 1. Construction Process of TPE-ADA/HACD Nanoparticle

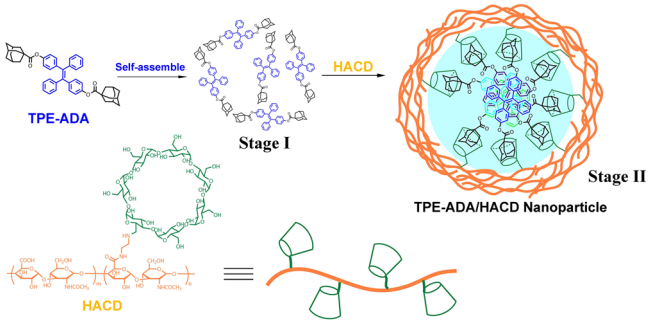

Then the hydrophilic **HA** shell of **TPE-ADA/HACD** nanoparticle could specially target HA-receptor positive cancer cells and realize the targeted fluorescent imaging toward cancer cells at the cellular level as well as presenting no cytotoxicity to both of cancer cells and normal cells. This work is considered as the great improvement of Qian Zhao et al.'s study,[28] where the synthetic step of **TPE** derivative was shorten from 4 (TPECD) to 2 (**TPE-ADA**), and **TPE-ADA/HACD** nanoparticle has greater fluorescence enhancement and quantum yield promotion than the TPECD-HAAD assembly. Therefore, cancer cell imaging could be realized by AIE effect of **TPE-ADA/HACD** without introducing other fluorescent agents. Compared with Bang-Ping Jiang et al.'s work,[29] the interaction between **HA** and **TPE** derivative was stronger by host−guest interaction in **TPE-ADA/HACD** than electrostatic interaction in QA-TPE/HA, and the cellular cytotoxicity could be greatly reduced without introducing positively charged tetraquaternary ammonium.

HACD was synthesized by hyaluronic acid (M_w = 190 000) and mono-6-deoxyl-6-ethylenediamino-β-CD in PBS according to the reported methods.[30,31] On the other hand, **TPE-ADA** was prepared from a facile two-step synthetic method containing nucleophilic substitution reaction and McMurry coupling reaction,[32] which were relatively simple and illustrated in Figure S1. The characterization of reaction intermediates and final **TPE-ADA** product by ^{1}H/^{13}C NMR spectroscopy and mass spectra were presented in Figures S2−S7. Moreover, it is obvious to find that *cis*−*trans* isomerism would exist in **TPE-ADA** fabrication. In this study, two fluorescent white solids with similar polarity and ^{1}H NMR spectra were separated from column chromatography. The less polar one had higher yield (45.2%), which was believed to be *trans*-isomer of **TPE-ADA** due to less steric hindrance than the *cis*-isomer. The higher polar one with 1.7% yield was assigned to the *cis*-isomer. Similar results could be also found in previous studies.[33,34] On the other hand, through theoretical simulation by Materials Studio 6.0, the *cis*-isomer indeed had a larger dipole (5.15 D, Figure S8a) than the *trans*-isomer (3.69 D, Figure S8b), and the *trans*-isomer had a higher melting point (341−342 °C) than the *cis*-isomer (310−311 °C) because the *cis*-isomers destroyed the molecular accumulation and were facile to be disorganized when the temperature increased. Therefore, *trans*-isomer and *cis*-isomer of **TPE-ADA** could be assigned, and the *trans*-isomer of **TPE-ADA** was employed as guest molecule in the following experiments.

Because of the hydrophobic nature of **TPE-ADA**, it tended to self-assemble in aqueous solution. Figure S9a exhibited amorphous structures in a high resolution transmission electron microscope (HR-TEM) image, indicating that **TPE-ADA** assembled in an incompact way. Dynamic light scattering (DLS, Figure S9b) revealed that the hydrodynamic diameter of **TPE-ADA** assembly was around 262 nm, which also presented ζ potential as +0.72 mV on the assembly's surface (Figure S9c). Therefore, **TPE-ADA** could form amorphous assembly with slightly positive charged surface in aqueous solution as stage I.

By utilizing the strong supramolecular interaction between adamantane groups and β-CD cavities, **HACD** was added into **TPE-ADA** to form supramolecular nanoparticle **TPE-ADA/HACD** in aqueous solution as stage II, where **TPE-ADA** was employed as typical molecule with AIE properties, and **HACD** was employed as targeting units for cancer cell recognition. As shown in Figure S10, in a typical Job's plot, a maximum value was observed at fraction ratio of 0.33, revealing the binding stoichiometry between **TPE-ADA** and β-CD was 1:2. Two adamantane groups in **TPE-ADA** could be included into cavities of two individual β-CD due to the supramolecular interaction. Next, the morphology and nanostructure of **TPE-ADA/HACD** were systematically investigated by atomic force microscope (AFM), HR-TEM, DLS, and ζ potential experiments. As shown in Figure 1a, a series of discrete spherical nanoparticles was observed in a typical AFM image. The average height of collapsed nanoparticle was measured as 5.8 nm, which was basically equal to the sum of two **HA** backbones (ca. 1.5 nm), two β-CD units, which included adamantane groups (ca. 2.0 nm), and anchored tetraphenylethene cores (ca. 2.0 nm). The HR-TEM image in Figure 1b also exhibited well-dispersed **TPE-ADA/HACD** nanoparticles, whose diameters were about 30−50 nm. Furthermore, the DLS experiment (Figure 1c) was performed to measure the hydrodynamic diameter of **TPE-ADA/HACD** as ∼84 nm, which was in accordance with the results of the HR-TEM image indicating good dispersity of nanoparticles in aqueous solution. To acquire more structural information about **TPE-ADA/HACD** nanoparticles, ζ potential experiment was employed to detect the charge distribution on nanoparticles' surface. As shown in Figure S11, the ζ potential of **TPE-ADA/HACD** was measured as −18.4 mV, indicating that the **TPE-ADA/HACD** nanoparticles were covered by negative charged **HA** shell owing to the ionization of carboxyl groups on the **HA** skeleton.

https://dx.doi.org/10.1021/acsmedchemlett.9b00559
ACS Med. Chem. Lett. 2020, 11, 451−456

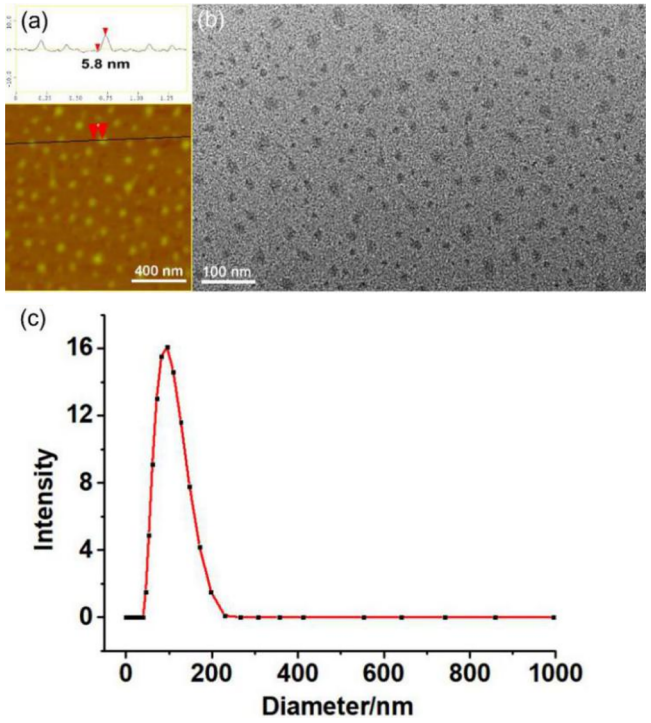

Figure 1. Typical (a) AFM, (b) HR-TEM, and (c) DLS results of **TPE-ADA/HACD** nanoparticles.

Besides, the elemental composition of **TPE-ADA** assembly in stage I and **TPE-ADA/HACD** nanoparticles in stage II was also measured by X-ray photoelectron spectroscopy (XPS, Figure S12). Only C (87.95 at%) and O (12.05 at%) elements could be found in **TPE-ADA** assembly. After the addition of **HACD**, due to abundant hydroxyl and carboxyl groups on the nanoparticle's surface, the content of O increased to 30.69 at%, the content of C decreased to 65.60 at%, and the element N appeared as 3.71 at% deriving from acetyl amino group on **HACD**. Therefore, HA skeleton was considered as the cover shell of **TPE-ADA/HACD** nanoparticles. Together with morphology comparison of **TPE-ADA** assembly and **TPE-ADA/HACD** nanoparticles, the addition of **HACD** could greatly change the assembly strategy of **TPE-ADA**, and the second stage nanoparticle **TPE-ADA/HACD** possessed good stability, dispersibility, and biocompatibility in the biological environment. Also, the negative charged HA shell could also promote the targeting of **TPE-ADA/HACD** nanoparticles toward cancer cells.

After successful construction of **TPE-ADA** assembly and **TPE-ADA/HACD** nanoparticle, we performed UV/vis and fluorescent spectra to investigate their photophysical properties. As shown in Figure S13, **HACD** showed almost no UV/vis absorption in the range from 250 to 800 nm, and **TPE-ADA** assembly exhibited maximum absorption peak at λ = 263 nm, which was assigned to $\pi-\pi^*$ electronic transitions of the **TPE-ADA** skeleton.[16] Besides, the shoulder peak at λ = 330 nm was observed. After adding **HACD** into **TPE-ADA**, the obtained **TPE-ADA/HACD** supramolecular nanoparticle gave similar UV/vis spectra, where a maximum absorption peak appeared at λ = 262 nm. This phenomenon revealed that the incorporation of **HACD** did not extremely change the energy level state of **TPE-ADA** in aqueous solution.

For further study of supramolecular AIE effect of **TPE-ADA**, fluorescent spectra were employed to investigate the aggregation behavior of **TPE-ADA** assembly and **TPE-ADA/HACD** nanoparticle. Figure S14 presented the fluorescence excitation spectrum of **TPE-ADA**, and 330 nm was selected as the excitation wavelength for fluorescence experiments. As shown in Figure S15a, when the concentration of **TPE-ADA** increased from 1×10^{-6} M to 5×10^{-5} M by 50-fold in pure DMSO, almost no fluorescence was observed from 350 to 650 nm, indicating that no AIE occurred for **TPE-ADA** in DMSO. However, at the same **TPE-ADA** concentration as 3×10^{-5} M, the fluorescence intensity of **TPE-ADA** at λ_{em} = 460 nm in aqueous solution containing 4% DMSO was 110-fold higher than that in pure DMSO solution (Figure S15b). In pure DMSO solution as good solvent, **TPE-ADA** existed as monomeric form to display feeble emission due to the intramolecular rotation of aromatic rings.[35] When water was added at fraction of 96 vol % as the nonsolvent, the **TPE-ADA** molecules aggregated, and the rotation of aromatic rings of **TPE-ADA** was restricted in aggregation, and then the fluorescence intensity was enhanced, which was typically called AIE phenomenon.[33,34]

As shown in Figure 2, under excitation wavelength of λ_{ex} = 330 nm, **HACD** showed no fluorescence, and **TPE-ADA**

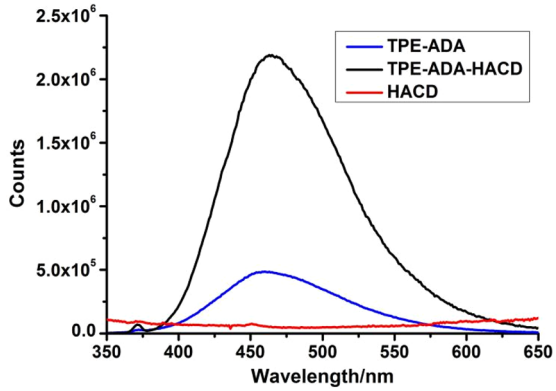

Figure 2. Fluorescent spectra of **HACD**, **TPE-ADA**, and **TPE-ADA/HACD** nanoparticle (λ_{ex} = 330 nm, [**TPE-ADA**] = 3×10^{-5} M, [**HACD**] = 8.8×10^{-7} M, containing 6×10^{-5} M β-CD, solvent was aqueous solution containing 4% DMSO at 25 °C).

exhibited a weak aggregation-induced fluorescent peak at λ_{em} = 460 nm. The relatively weak AIE phenomenon of **TPE-ADA** could be attributed to the poor solubility nature and self-aggregation impediment of the tetraphenylethene group of **TPE-ADA** in aqueous solution. Because the hydrophobic adamantane group in **TPE-ADA** would have the same trend to self-assemble and compete with π stacking of the tetraphenylethene group, then incompact **TPE-ADA** assembly formed with low AIE effect at the first stage. After addition of **HACD**, the hydrophobic adamantane group was included by β-CD of **HACD** and turned hydrophilic, and then the $\pi-\pi$ stacking in **TPE** core and restriction of adamantane group by **HACD** together restrained the intramolecular motions (including rotation and vibration) of phenyl groups and increased the rigidity of tetraphenylethene,[36,37] which reduced the non-radiative decay with turn-on AIE emission. Therefore, the fluorescent intensity of **TPE-ADA/HACD** nanoparticle increased by 4.5-times at the second stage (λ_{em} = 465 nm) compared with **TPE-ADA** assembly.

On the other hand, the turn-on AIE emission was accompanied by variation in fluorescence lifetime and

https://dx.doi.org/10.1021/acsmedchemlett.9b00559
ACS Med. Chem. Lett. 2020, 11, 451−456

fluorescence quantum yield. As shown in Figure S16, after addition of **HACD**, the lifetime of **TPE-ADA/HACD** (4.60 ns, χ^2 = 1.10) was slightly increased compared with **TPE-ADA** assembly (3.96 ns, χ^2 = 1.09), but the quantum yield was greatly enhanced (from Φ = 17.88% of **TPE-ADA** to Φ = 66.07% of **TPE-ADA/HACD**).

Combined with the results in ζ potential experiment (Figure S11), which indicated negative charge existence on **TPE-ADA/HACD** nanoparticle surface, we could affirm that **TPE-ADA/HACD** nanoparticle was composed of hydrophilic **HA** shell and hydrophobic tetraphenylethene core, which could give enhanced AIE effect compared with **TPE-ADA** self-aggregation. Furthermore, the two-stage enhancement of AIE effect by **TPE-ADA** and **TPE-ADA/HACD** formation can be distinguished by naked eyes. As shown in Figure S17, the prepared **TPE-ADA** powder exhibited obvious solid fluorescence under UV light (365 nm) due to the AIE effect of **TPE-ADA** in solid state. However, as shown in Figure 3a,

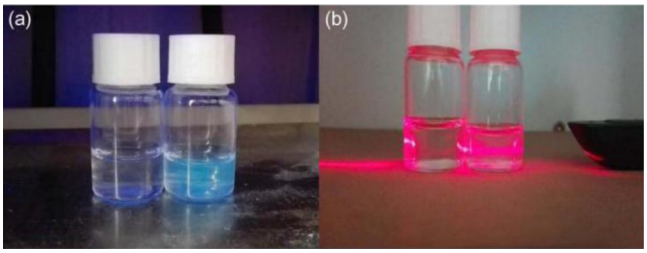

Figure 3. (a) Fluorescent image of **TPE-ADA** (left) and **TPE-ADA/HACD** (right); (b) Tyndall effects of **HACD** (left) and **TPE-ADA/HACD** (right).

compared with weak fluorescent intensity of **TPE-ADA** assembly at the first stage in aqueous solution, the second-stage enhancement of AIE effect was realized for **TPE-ADA/HACD** nanoparticles, which was in accordance with Figure 2. On the other, the promoted Tyndall phenomenon could be also observed after addition of **TPE-ADA** into **HACD** aqueous solution (Figure 3b), further proving the formation of **TPE-ADA/HACD** nanoparticle with nanosize.

Taking advantage of AIE effect and targeted **HA** shell of **TPE-ADA/HACD** nanoparticle, fluorescent confocal experiments by **TPE-ADA/HACD** nanoparticles using HA-receptor positive PC-3 human prostate cancer cells and HA-receptor negative NIH3T3 mouse embryonic fibroblasts were performed. As shown in Figure 4, after incubation with **TPE-ADA/HACD** nanoparticle for 4 h, PC-3 cells exhibited bright blue fluorescence assigned to AIE effect, revealing that **TPE-ADA/HACD** nanoparticles were relative stable *in vitro* and successfully delivered into cancer cells by HA-receptor mediated endocytosis. In contrast, lacking HA-receptor on the cell membrane, no fluorescence was observed in NIH3T3 cells under the same experimental condition. All the experimental phenomena testified that **TPE-ADA/HACD** nanoparticles could be applied for cancer cell imaging with high efficiency, which was ascribed to the specific **TPE-ADA/HACD** nanoparticle's structure of hydrophilic **HA** shell with cancer cell targeting function, and hydrophobic tetraphenylethene core with AIE effect.

For the purpose of studying the safety of **TPE-ADA/HACD** nanoparticle in application of cancer cell imaging, cytotoxicity experiments were performed through incubation of PC-3 cancer cells and NIH3T3 cells with **TPE-ADA/HACD**

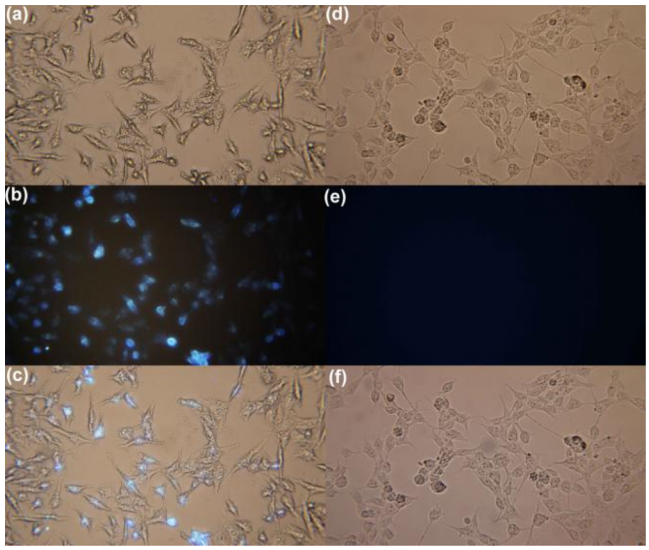

Figure 4. Fluorescent confocal images of PC-3 cells in (a) bright field, (b) dark field, (c) merged field; NIH3T3 cells in (d) bright field, (e) dark field, (f) merged field after incubation with **TPE-ADA/HACD** nanoparticles for 4 h (containing 5×10^{-5} M **TPE-ADA** and 1×10^{-4} M β-CD).

nanoparticles for 24 and 48 h by CCK8 assay. As shown in Figure 5, after incubation with **TPE-ADA/HACD** nano-

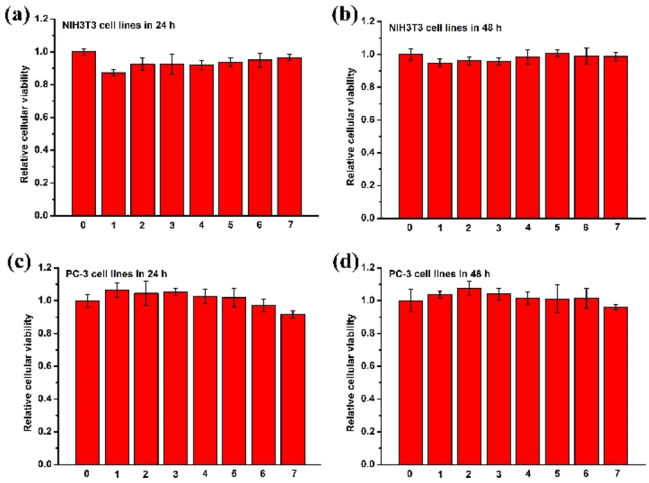

Figure 5. Cytotoxicity experiments of NIH3T3 cells (a) in 24 h, (b) in 48 h, and PC-3 cells (c) in 24 h, (d) in 48 h after incubation with **TPE-ADA/HACD** nanoparticles with different concentrations ([**TPE-ADA**] = 0, 2.06, 6.17, 18.5, 55.5, 167, 500, 1500 μM).

particles with different concentrations ([**TPE-ADA**] = 0, 2.06, 6.17, 18.5, 55.5, 167, 500, 1500 μM) for 24 and 48 h, respectively, no cytotoxicity could be observed on both normal NIH3T3 cells and PC-3 cancer cells, whose cellular viability completely exceeded 95%. These experimental results proved that even high concentration of **TPE-ADA/HACD** nanoparticles would not damage the cytomembrane and organelle of normal cells or cancer cells and was safe and biocompatible enough for cancer cell imaging application.

In conclusion, a novel supramolecular nanoparticle bearing **TPE-ADA** and **HACD** was successfully constructed via host–guest interactions, which exhibited enhanced AIE effect mediated in two stages. The obtained **TPE-ADA/HACD**

https://dx.doi.org/10.1021/acsmedchemlett.9b00559
ACS Med. Chem. Lett. 2020, 11, 451–456

nanoparticle could specifically target cancer cells through HA−HA receptor interactions and emit blue fluorescence *in vitro* to distinguish cancer cells from normal cells without introducing obvious side effects. The supramolecular construction strategy in this study would be applied for multiple cancer cell imaging and recognition.

■ ASSOCIATED CONTENT

Supporting Information

The Supporting Information is available free of charge at https://pubs.acs.org/doi/10.1021/acsmedchemlett.9b00559.

Experimental details, compounds characterization, theoretical simulation, **TPE-ADA** assembly characterization, Job's plot, ζ potential, XPS spectra, fluorescence characterization results (PDF)

■ AUTHOR INFORMATION

Corresponding Author

Yu Liu − *Department of Chemistry, State Key Laboratory of Elemento-Organic Chemistry, Nankai University, Tianjin 300071, P. R. China;* orcid.org/0000-0001-8723-1896; Email: yuliu@nankai.edu.cn

Authors

Yang Yang − *School of Chemical Engineering and Technology, Hebei University of Technology, Tianjin 300130, P. R. China*

Ya-Jun Jin − *School of Chemical Engineering and Technology, Hebei University of Technology, Tianjin 300130, P. R. China*

Xin Jia − *School of Chemical Engineering and Technology, Hebei University of Technology, Tianjin 300130, P. R. China*

Shi-Kuo Lu − *School of Chemical Engineering and Technology, Hebei University of Technology, Tianjin 300130, P. R. China*

Ze-Rui Fu − *School of Chemical Engineering and Technology, Hebei University of Technology, Tianjin 300130, P. R. China*

Yu-Xi Liu − *School of Chemical Engineering and Technology, Hebei University of Technology, Tianjin 300130, P. R. China*

Complete contact information is available at: https://pubs.acs.org/10.1021/acsmedchemlett.9b00559

Notes

The authors declare no competing financial interest.

■ ACKNOWLEDGMENTS

We thank the NNSFC (21871154, 21772099, and 21402038) and the Hebei Provincial Natural Science Foundation of China (B2015202291 and B2019202003) for financial support.

■ REFERENCES

(1) Chen, X.-M.; Chen, Y.; Yu, Q.; Gu, B.-H.; Liu, Y. Supramolecular Assemblies with Near-infrared Emission Mediated in Two Stages by Cucurbituril and Amphiphilic Calixarene for Lysosome-targeted Cell Imaging. *Angew. Chem., Int. Ed.* **2018**, *57*, 12519−12523.

(2) Zhang, J.; Wang, Q.; Guo, Z.; Zhang, S.; Yan, C.; Tian, H.; Zhu, W.-H. High-fidelity Trapping of Spatial-temporal Mitochondria with Rational Design of Aggregation-induced Emission Probes. *Adv. Funct. Mater.* **2019**, *29*, 1808153.

(3) Tang, B. Z.; Zhan, X.; Yu, G.; Lee, P. P. S.; Liu, Y.; Zhu, D. J. Efficient Blue Emission from Siloles. *J. Mater. Chem.* **2001**, *11*, 2974−2978.

(4) Zheng, J.; Ye, T.; Chen, J.; Xu, L.; Ji, X.; Yang, C.; He, Z. Highly Sensitive Fluorescence Detection of Heparin based on Aggregation-Induced Emission of a Tetraphenylethene Derivative. *Biosens. Bioelectron.* **2017**, *90*, 245−250.

(5) Chen, Y.; Lam, J. W. Y.; Kwok, R. T. K.; Liu, B.; Tang, B. Z. Aggregation-induced Emission: Fundamental Understanding and Future Developments. *Mater. Horiz.* **2019**, *6*, 428−433.

(6) Mei, J.; Leung, N. L. C.; Kwok, R. T. K.; Lam, J. W. Y.; Tang, B. Z. Aggregation-induced Emission: Together We Shine, United We Soar. *Chem. Rev.* **2015**, *115*, 11718−11940.

(7) Hong, Y.; Lam, J. W. Y.; Tang, B. Z. Aggregation-induced Emission. *Chem. Soc. Rev.* **2011**, *40*, 5361−5388.

(8) Shi, X.; Yu, C. Y. Y.; Su, H.; Kwok, R. T. K.; Jiang, M.; He, Z.; Lam, J. W. Y.; Tang, B. Z. A Red-emissive Antibody-AIEgen Conjugate for Turn-on and Wash-free Imaging of Specific Cancer Cells. *Chem. Sci.* **2017**, *8*, 7014−7024.

(9) Gao, M.; Su, H.; Lin, G.; Li, S.; Yu, X.; Qin, A.; Zhao, Z.; Zhang, Z.; Tang, B. Z. Targeted Imaging of EGFR Overexpressed Cancer Cells by Brightly Fluorescent Nanoparticles Conjugated with Cetuximab. *Nanoscale* **2016**, *8*, 15027−15032.

(10) Liang, G. D.; Lam, J. W. Y.; Qin, W.; Li, J.; Xie, N.; Tang, B. Z. Molecular Iuminogens based on Restriction of Intramolecular Motions Through Host-guest Inclusion for Cell Imaging. *Chem. Commun.* **2014**, *50*, 1725−1727.

(11) Gao, M.; Su, H.; Lin, Y.; Ling, X.; Li, S.; Qin, A.; Tang, B. Z. Photoactivatable Aggregation-induced Emission Probes for Lipid Droplets-specific Live Cell Imaging. *Chem. Sci.* **2017**, *8*, 1763−1768.

(12) Yang, Y.; Zhang, Y.-M.; Chen, Y.; Chen, J.-T.; Liu, Y. Polysaccharide-based Noncovalent Assembly for Targeted Delivery of Taxol. *Sci. Rep.* **2016**, *6*, 19212.

(13) Zhang, Y.-H.; Zhang, Y.-M.; Zhao, Q.-H.; Liu, Y. Simultaneous Expression and Transportation of Insulin by Supramolecular Polysaccharide Nanocluster. *Sci. Rep.* **2016**, *6*, 22654.

(14) Zhang, Y.-H.; Zhang, Y.-M.; Yang, Y.; Chen, L.-X.; Liu, Y. Controlled DNA Condensation and Targeted Cellular Imaging by Ligand Exchange in a Polysaccharide-quantum Dot Conjugate. *Chem. Commun.* **2016**, *52*, 6087−6090.

(15) Zhao, Q.; Chen, Y.; Liu, Y. A Polysaccharide/Tetraphenylethylene-mediated Blue-Light Emissive and Injectable Supramolecular Hydrogel. *Chin. Chem. Lett.* **2018**, *29*, 84−86.

(16) Yu, J.; Chen, Y.; Zhang, Y.-H.; Xu, X.; Liu, Y. Supramolecular Assembly of Coronene Derivatives for Drug Delivery. *Org. Lett.* **2016**, *18*, 4542−4545.

(17) Rodell, C. B.; Rai, R.; Faubel, S.; Burdick, J. A.; Soranno, D. E. J. Local Immunotherapy via Delivery of Interleukin-10 and Transforming Growth Factor β Antagonist for Treatment of Chronic Kidney Disease. *J. Controlled Release* **2015**, *206*, 131−139.

(18) Oommen, O. P.; Duehrkop, C.; Nilsson, B.; Hilborn, J.; Varghese, O. P. Multifunctional Hyaluronic Acid and Chondroitin Sulfate Nanoparticles: Impact of Glycosaminoglycan Presentation on Receptor Mediated Cellular Uptake and Immune Activation. *ACS Appl. Mater. Interfaces* **2016**, *8*, 20614−20624.

(19) Zhang, Y.-M.; Xu, Q.-Y.; Liu, Y. Molecular Recognition and Biological Application of Modified β-Cyclodextrins. *Sci. China: Chem.* **2019**, *62*, 549−560.

(20) Chen, Z.; Liu, W.; Zhao, L.; Xie, S.; Chen, M.; Wang, T.; Li, X. Acid-labile Degradation of Injectable Fiber Fragments to Release Bioreducible Micelles for Targeted Cancer Therapy. *Biomacromolecules* **2018**, *19*, 1100−1110.

(21) Li, X.; Zhou, Z.; Tang, Y.; Zhang, C. C.; Zheng, Y.; Gao, J.; Wang, Q. Modulation of Assembly and Disassembly of a New Tetraphenylethene based Nanosensor for Highly Selective Detection of Hyaluronidase. *Sens. Actuators, B* **2018**, *276*, 95−100.

(22) Wang, X.; Li, Y.; Li, Q.; Neufeld, C. I.; Pouli, D.; Sun, S.; Yang, L.; Deng, P.; Wang, M.; Georgakoudi, I.; Tang, S.; Xu, Q. J. Hyaluronic Acid Modification of RNase A and its Intracellular Delivery using Lipid-like Nanoparticles. *J. Controlled Release* **2017**, *263*, 39−45.

(23) Thomas, A. P.; Palanikumar, L.; Jeena, M. T.; Kim, K.; Ryu, J. H. Cancer-mitochondria-targeted Photodynamic Therapy with Supramolecular Assembly of HA and a Water Soluble NIR Cyanine Dye. *Chem. Sci.* **2017**, *8*, 8351−8356.

(24) Zhou, B.; Jiang, B.-P.; Sun, W.; Wei, F.-M.; He, Y.; Liang, H.; Shen, X.-C. Water-dispersible Prussian Blue Hyaluronic Acid Nanocubes with Near-infrared Photoinduced Singlet Oxygen Production and Photothermal Activities for Cancer Theranostics. *ACS Appl. Mater. Interfaces* **2018**, *10*, 18036−18049.
(25) Luo, Y.; Prestwich, G. D. Synthesis and Selective Cytotoxicity of a Hyaluronic Acid-antitumor Bioconjugate. *Bioconjugate Chem.* **1999**, *10*, 755−763.
(26) Park, K. M.; Yang, J.-A.; Jung, H.; Yeom, J.; Park, J. S.; Park, K.-H.; Hoffman, A. S.; Hahn, S. K.; Kim, K. In situ Supramolecular Assembly and Modular Modification of Hyaluronic Acid Hydrogels for 3D Cellular Engineering. *ACS Nano* **2012**, *6*, 2960−2968.
(27) Lee, M.-Y.; Park, S.-J.; Park, K.; Kim, K. S.; Lee, H.; Hahn, S. K. Target-specific Gene Silencing of Layer-by-layer Assembled Gold-cysteamine/siRNA/PEI/HA Nanocomplex. *ACS Nano* **2011**, *5*, 6138−6147.
(28) Zhao, Q.; Chen, Y.; Sun, M.; Wu, X.-J.; Liu, Y. Construction and Drug Delivery of a Fluorescent TPE-bridged Cyclodextrin/Hyaluronic Acid Supramolecular Assembly. *RSC Adv.* **2016**, *6*, 50673−50679.
(29) Jiang, B.-P.; Tan, X.-Y.; Shen, X.-C.; Lei, W.-Q.; Liang, W.-Q.; Ji, S.-C.; Liang, H. One-step Fabrication of a Multifunctional Aggregation-induced Emission Nanoaggregate for Targeted Cell Imaging and Enzyme-triggered Cancer Chemotherapy. *ACS Macro Lett.* **2016**, *5*, 450−454.
(30) May, B. L.; Kean, S. D.; Easton, C. J.; Lincoln, S. F. Preparation and Characterization of 6(A)-Polyamine-mono-substituted Beta-cyclodextrins. *J. Chem. Soc., Perkin Trans. 1* **1997**, 3157−3160.
(31) Yang, Y.; Zhang, Y.-M.; Chen, Y.; Chen, J.-T.; Liu, Y. Targeted Polysaccharide Nanoparticle for Adamplatin Prodrug Delivery. *J. Med. Chem.* **2013**, *56*, 9725−9736.
(32) Xie, H.; Zeng, F.; Yu, C.; Wu, S. A Polylysine-based Fluorescent Probe for Sulfite Anion Detection in Aqueous Media via Analyte-induced Charge Generation and Complexation. *Polym. Chem.* **2013**, *4*, 5416−5424.
(33) Peng, W.; Li, L.; Zheng, S. Photoluminescent Epoxy Microspheres: Preparation, Surface Functionalization via Grafting Polymerization and Photophysical Properties. *RSC Adv.* **2015**, *5*, 77922−77931.
(34) Shi, H.; Gong, Z.; Xin, D.; Roose, J.; Peng, H.; Chen, S.; Lam, J. W. Y.; Tang, B. Z. Synthesis, Aggregation-induced Emission and Electroluminescence Properties of a Novel Compound Containing Tetraphenylethene, Carbazole and Dimesitylboron Moieties. *J. Mater. Chem. C* **2015**, *3*, 9095−9102.
(35) Chu, N.-T.; Chakravarthy, R. D.; Shih, N.-C.; Lin, Y.-H.; Liu, Y.-C.; Lin, J.-H.; Lin, H.-C. Fluorescent Supramolecular Hydrogels Self-assembled from Tetraphenylethene (TPE)/Single Amino Acid Conjugates. *RSC Adv.* **2018**, *8*, 20922−20927.
(36) Zhang, F.; Fan, J.; Yu, H.; Ke, Z.; Nie, C.; Kuang, D.; Shao, G.; Su, C. Nonplanar Organic Sensitizers Featuring a Tetraphenylethene Structure and Double Electron-withdrawing Anchoring Groups. *J. Org. Chem.* **2015**, *80*, 9034−9040.
(37) Jiang, B.-P.; Guo, D.-S.; Liu, Y.-C.; Wang, K.-P.; Liu, Y. Photomodulated Fluorescence of Supramolecular Assemblies of Sulfonatocalixarenes and Tetraphenylethene. *ACS Nano* **2014**, *8*, 1609−1618.

https://dx.doi.org/10.1021/acsmedchemlett.9b00559
ACS Med. Chem. Lett. 2020, 11, 451−456